Electrorotation of single microalgae cells during lipid accumulation for assessing cellular dielectric properties and total lipid contents

Yu-Sheng Lin, Sung Tsang, Sakina Bensalem, Ching-Chu Tsai, Shiang-Jiuun Chen, Chen-Li Sun, Filipa Lopes, Bruno Le Pioufle, Hsiang-Yu Wang

Electrorotation of single microalgae cells during lipid accumulation for assessing cellular dielectric properties and total lipid contents

Yu-Sheng Lin[1,3], Sung Tsang[2], Sakina Bensalem[3,6], Ching-Chu Tsai[5], Shiang-Jiuun Chen[5], Chen-li Sun[2], Filipa Lopes[6], Bruno Le Pioufle[4], Hsiang-Yu Wang*[,1]

[1]Department of Engineering and System Science, National Tsing Hua University, Hsinchu, Taiwan
[2]Department of Mechanical Engineering, National Taiwan University, Taipei 10617, Taiwan
[3]ENS Paris Saclay, CNRS Institut d'Alembert, SATIE, Université Paris Saclay, 91192 Gif sur Yvette, France
[4]ENS Paris Saclay, CNRS Institut d'Alembert, LUMIN, Université Paris Saclay, 91192 Gif sur Yvette, France
[5]Institute of Ecology and Evolutionary Biology, National Taiwan University, Taipei 10617, Taiwan
[6]CentraleSupélec, LGPM, Université Paris Saclay, 91192 Gif-sur-Yvette Cedex, France

* Correspondence: hywang@ess.nthu.edu.tw; Tel.: +886-5715131 ext 34243

Abstract

Photosynthetic microalgae not only perform fixation of carbon dioxide but also produce valuable byproducts such as lipids and pigments. However, due to the lack of effective tools for rapid and noninvasive analysis of microalgal cellular contents, the efficiency of strain screening and culture optimizing is usually quite low. This study applied single-cell electrorotation on *Scenedesmus abundans* to assess cellular dielectric properties during lipid accumulation and to promptly quantify total cellular contents. The experimental electrorotation spectra were fitted with the double-shell ellipsoidal model, which considered varying cell wall thickness, to obtain the dielectric properties of cellular compartments. When the amount of total lipids increased from 15.3 wt% to 33.8 wt%, the conductivity and relative permittivity of the inner core (composed of the cytoplasm, lipid droplets, and nucleus) decreased by 21.7 % and 22.5 %, respectively. These dielectric properties were further used to estimate total cellular lipid contents by the general mixing formula, and the estimated values agree with those obtained by weighing dry biomass and extracted lipids with an error as low as 0.22 wt%. Additionally, the conductivity and relative permittivity of the cell wall increased as the nitrogen-starvation period increased, indicating the thickening of cell wall, which was validated by the TEM images.

Keywords

Electrorotation, Microalgae, Total lipid contents, Cell wall properties, Permittivity, Conductivity

1. Introduction

Biofuel production from renewable feedstock such as microalgae has received wide attention and intense research efforts for enhancing the efficiency and productivity (Mata, Martins, and Caetano 2010; Medipally et al. 2015). Microalgae are pho

tosynthetic microorganisms that produce lipids and carbohydrates through “fixing” carbon dioxide with the aid of light (Xu et al. 2019) and therefore microalgal biofuel production has a great potential to achieve carbon neutrality. High conversion efficiency of carbon dioxide into lipids is critical in increasing the CO_2 utilization rate and reducing the production costs. To date, many efforts have been made to study the effects of various cultivation strategies on the enhancement of microalgal biofuels and biorefinery industry (Breuer et al. 2013; Chen et al. 2017). Environmental stresses such as nitrogen starvation, high salinity, and high light intensities are commonly applied to induce the accumulation of cellular lipids (Rai and Gupta 2017). However, the efficacy of these stresses in enhancing lipid productivity is species and strain dependent. Additionally, the evaluation of the efficacy is usually slow because conventional methods for analyzing intracellular contents are either time-consuming or strain-sensitive (T. H. Lee, Chang, and Wang 2013; Patel et al. 2019). The presence of the microalgal cell wall makes cellular lipid quantification a complex and tedious process because the extraction of cellular lipids requires effective disruption of the cell wall. The whole process involves a harvesting, drying, cell disruption, and lipid extraction step which may take up to days. Moreover, the process requires customization for different microalgal strains (Li et al. 2014). Microalgal cellular contents vary significantly during the nutrient-depletion process and low productivity is highly possible if the harvest timing is not optimized. Therefore, a rapid quantification method for the total cellular lipid content is essential in ensuring a satisfactory productivity.

Recently, several high-throughput analysis methods for microalgal lipids were developed, such as fluorescence spectroscopy, Fourier transform infrared spectroscopy (FTIR), Raman spectroscopy, and dielectric spectrometry (T. H. Lee, Chang, and Wang 2013; Patel et al. 2019). (Rumin et al. 2015) reviewed the fluorescence staining of microalgal lipids and addressed several limitations such as aggregated fluorochrome, species-dependent dye concentrations, and changeable incubation durations due to the variation of cell wall compositions. Without preliminary work to optimize the protocol, (Rumin et al. 2015) pointed out that fluorescence labeling of lipids can lead to quantification errors. Moreover, optimal staining protocol also depends on the physiological status of microalgae which can change rapidly during the nutrient-depletion process. (Dean et al. 2010) proposed the use of FTIR to determine microalgal lipid contents in a time series and validated the outcomes with the quantification by fluorescence spectroscopy. Nevertheless, FTIR required sample drying and continuation of cell culture was impossible after the examination. Raman spectroscopy provided a rapid and non-invasive way to quantify average cellular lipids of a bulk sample (T.-H. Lee, Chang, and Wang 2013) or single microalgal cells (H. Wu et al. 2011). Although *in vivo* lipid detection was demonstrated on bulk microalgal samples, cells with high lipid abundance could not be separated from others for further cultivation and refinement. On the other hand, bleaching of cellular pigments was necessary for single-cell measurement to improve the signal-to-noise ratio but cell viability decreased significantly afterwards.

Dielectric spectrometry used intrinsic cell properties such as permittivity and conductivity of cellular components to characterize cell status. The evolution of the cellular dielectric properties could be measured through bioimpedance, dielectrophoresis, and electrorotation. Bioimpedance measurement has been widely applie

d to study the microalgae vitality and cellular lipid abundances (Saqer et al. 2015; Martínez-Bisbal et al. 2019; Sui et al. 2020). In (Martínez-Bisbal et al. 2019), impedance spectroscopy accompanying with voltammetric electronic tongue and NMR spectroscopy were used to monitor the status of microalgae (*Nannochloropsis oceanica*) during growth and the results can be further used as the reference in real-time monitoring of microalgal quality. In addition, electrical impedance can be an indicator of microalgal health and provides information of cellular phenotypes such as cell size (Sui et al. 2020). (Saqer et al. 2015) proposed an impedance-based technique to predict cellular lipid contents by the change of impedance phase and the phase decreased exponentially from around -65° to -90° while the lipid content increased from around 10 wt% to 70 wt%. However, the impedance of a sample was highly dependent on the volume fraction of cells, making single cell measurement challenging. The changes in cellular lipid amounts modify the dielectric properties of microalgae and several reports used dielectrophoresis to sort microalgal cells with different total lipid contents (Schor and Buie 2012; Deng, Kuo, and Juang 2014; Hadady et al. 2014, 2016). In (Deng, Kuo, and Juang 2014), microalgae cells (*C. vulgaris*) with average lipid contents of 13 wt% and 21 wt% were separated by dielectrophoresis force at 7 MHz, using a low conductivity of buffer (2.93 mS/cm). These results showed that the difference in dielectric behavior enabled the selection of microalgae cells based on their total lipid contents. However, the suitable separation parameters can only be determined by trial and error. These parameters were also sensitive to microalgae species and operational conditions such as the conductivities of solutions. Although dielectrophoresis could be utilized to differentiate cells with high and low lipid abundances, accurate lipid quantification is yet to be realized. Similarly, the characterization of microalgae using such techniques remains challenging. Electrorotation provides direct measurements of complex permittivity (relative permittivity and conductivity) of cells which is very beneficial for the fundamental biological researches and the measurement is independent of the volume of the measured chamber and cell density (Français and Le Pioufle 2017). The obtained complex permittivity from electrorotation can be used to differentiate different cell types and could be further used on the research of cancers (Kawai et al. 2020; Huang et al. 2020). In (Claudia I. Trainito et al. 2019), electrorotation is used to exploit sequentially-staged cancer cells and determine the differences of complex permittivity between malignant cells and non-malignant cells. Electrorotation technique was also used on microalgae. Single microalgae cells were suspended in droplets and rotated by four 90° -phase-shifted electric waves in (Müller, Schnelle, and Fuhr 1998) and the obtained electrorotation spectra were fitted by a multi-shell model to estimate the conductivities and permittivities of cell wall, cytoplasm, and cell membrane. Through the fitted dielectric properties, they found that the conductivity of inner core (cytoplasm and nucleus) was lower than the protoplast of higher plants due to leaking of ions to the low-conductivity snow water. The cell wall of snow algae also had a low permittivity which was attributed to the existence of Al-Fe silicates. Currently, electrorotation is the most informative dielectric spectrometry to understand the changes in cell dielectric properties, cell structures, and cellular compositions. However, only qualitative analyses of microalgae have been presented in existing studies (Y. Wu et al. 2005; Han, Huang, and Han 2019). Herein, the first application of electrorotation on the quantification of total cellular lipid content is demonstrated and validated. Addition

ally, the electrorotation spectra also indicate the thickening of cell wall during nitrogen starvation and the cell wall thickening is witnessed by transmission electron microscopy (TEM).

This study integrated dielectrophoresis and electrorotation techniques (Claudia Irene Trainito, Français, and Le Pioufle 2015) for the measurement of the dielectric properties and the estimation of the total lipid content in microalgal cells. Once trapped at the center of a set of electrodes by negative dielectrophoresis, the single microalgal cell was induced to rotate by applying a rotating electric field. The genetic algorithm (Johnson and Rahmat-Samii 1997) was employed to fit the measured electrorotation spectra with single-shell models. The fitted dielectric properties were then used to estimate the total cellular lipid content by the mixing theory and to understand the structural and compositional change of cell wall that was parallelly observed in *Scenedesmus abundans* cells during nitrogen starvation. The changes in terms of dielectric properties provide a better understanding of microalgae physiological status and valuable information for improving biofuel production processes. For example, the harvest timing for high lipid productivity can be determined by observing the conductivity of cytoplasm and the facilitated lipid extraction can be achieved by investigating the relative permittivity and conductivity of the cell wall.

2. Material and methods

2.1 Microalgae culture and nitrogen starvation

Scenedesmus abundans were cultured in modified CHU-13 medium (Mandotra et al. 2014) under a light intensity of 20 $\mu molm^{-2}s^{-1}$ and a shaking speed of 99 rpm in an incubator (Minitron, Infors HT, Bottmingen, Switzerland) to reach log phase with a cell concentration around 1×10^7 cells/ml (measured by Guava EasyCyte™ 8 Flow Cytometer, EMD Millipore). The temperature was held constant at 24.5 ° C and CO_2 supply was maintained at 1.5 % (v/v). In order to enhance the cellular lipid production, microalgae were then transferred to a nitrogen-free modified CHU-13 medium and kept under nitrogen-starved conditions (T.-H. Lee, Chang, and Wang 2013) for 7 days under a high light intensity of 150 $\mu molm^{-2}s^{-1}$.

2.2 Quantification of total lipid contents by single-step lipid extraction

Microalgae lipids were extracted according to the single-step lipid extraction reported in (Axelsson and Gentili 2014). Microalgal samples were centrifuged at 6000 g for 5 minutes and the pellet was placed on aluminum foil for drying overnight at 65 ° C in the oven. After weighing the dry biomass, the dried microalgal powder was then resuspended in 8 ml of a 2:1 chloroform-methanol (v/v) mixture and agitated at 99 rpm for 30 minutes. Afterwards, 2 ml of 0.73 wt% NaCl aqueous solution was blended in by agitating at 99 rpm for another 30 min. Chloroform-lipid mixture was separated from methanol-water mixture by 2 minutes of centrifugation at 350 g and recovered from the lower phase. The amount of total lipids was determined by weighing after chloroform was evaporated completely. The lipid content was calculated as:

$$Lipid\ content\ (wt\%) = \frac{lipids\ weight\ (g/L)}{dry\ cell\ weight\ (g/L)} \times 100\,\% \qquad (1)$$

2.3 Transmission electron microscopy (TEM)

The samples were fixed in 2.5 % glutaraldehyde in a 0.1 M phosphate buffer (pH = 6.8) for 2 hours, post fixed in buffered 1 % Osmium tetroxide for 1 hour, and then dehydrated in an acetone series. The samples were embedded in Spurr's resin (Spurr 1969) For TEM, thin sections were cut with an Ultracut E (Reichert, Inc., NY, USA), observed under Hitachi-7650 TEM, and pictures taken by CCD camera (Gatan ES500W Erlangshen).

2.4 Device fabrication

For the electrorotation experiment, a device with four planar hyperbolic electrodes was fabricated. The electrodes' shape follows the polynomial equation: $x^2 - y^2 = \pm d^2$, where d stands for the distance between the tip of electrode and the center of hyperbolic pair which a cell is trapped by negative dielectrophoresis (see figure 1a). In this study, 2d = 75 μm. Such shape is proven to produce an homogeneous electric field used for microalgae electrorotation (Claudia Irene Trainito, Français, and Le Pioufle 2015). The fabrication was achieved by conventional cleanroom technology. The electrodes were made on a 2-in quartz wafer on which a 150 nm gold layer was deposited by evaporation above a 20 nm chromium adhesion layer. Photoresist S1805 was patterned to serve as the etching mask of the metal layers, which was etched by potassium iodide solution and chromium etchant to reveal the electrode set on the quartz substrate. The fabricated electrodes and device are shown in figure 1a and figure 1b, respectively. A tape (3M) with a thickness around 50 μm was positioned on the topside of the electrode layer to define the height of the fluidic chamber for holding the microalgae sample. 3 sets of four polynomial electrodes were designed on the same device.

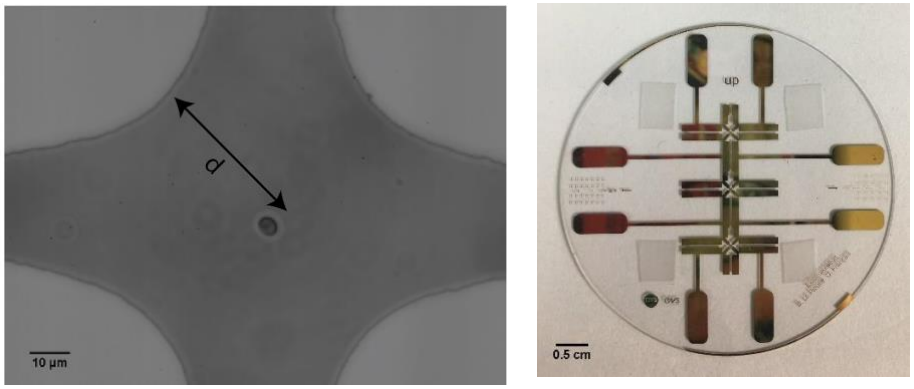

(a) (b)

Figure 1. Device for conducting electrorotation of single microalgae cells: (a) single microalgae cell (*S. abundans*) captured at the center of the microelectrode set; (b) the device overview.

2.5 Electrorotation

Cells with a concentration of 5×10^5 cells/ml were collected by centrifugation (6000 g, 5 minutes), washed three times in modified CHU-13 medium, and resuspended in modified CHU-13 medium with the conductivity adjusted to 0.12 S/m. The viability of microalgal cells in this solution is shown as figure S1. Microalgae sample with a volume of 50 μl was deposited on the device. To prevent evaporation, the device was then covered by a microscope cover glass (thickness t = 170 μm) with a di

mension of 24×60 mm (Deckglaser, Germany). After applying the negative dielectrophoretic force, single microalgae cells could be captured at the center of the microelectrode set as shown in figure 1a. By superimposing a rotating electric field, the trapped cell was brought into a rotational movement (rotation axis orthogonal to the plane of the substrate). The electrorotation measurement for one single cell was accomplished within 1 minute which minimizes any deletary effect of the electric field on microalgal cells. As shown in figure S2, electrorotation spectrum of microalgae, before and after high electric treatment, are almost the same which replied its dielectrophoresis characteristics remain the same.

The schematic of the experimental setup is depicted in figure 2. Two electric signals were superposed to trap and rotate the microalgal cells. The first electric signal was used to create a stationary electric field for the capture of the single microalgal cell and the electric field was produced by applying sinusoidal voltages to the four electrodes, adjacent electrodes being powered with 180° phase-shifted signals. The sinusoidal voltage was provided by the function generator (33250A, Agilent Technologies) and set at 3 Vpp amplitude and 1 MHz frequency. This stationary electric field produced negative dielectrophoresis (DEP) for trapping cells at the center of the four-electrodes set. The second electric signal provided a rotating electric field for electrorotation (ROT). For this purpose a second function generator (AFG 3102, Tektronix) was used to produce 3 Vpp amplitude voltages with 90° phase-shift between adjacent electrodes. The frequency of the latter signal was tuned in the range between 37 kHz and 25 MHz. The electric field for electrorotation along the Z-direction is shown in figure S3 and the cell did not levitate during the electrorotation experiment as shown in figure S4. A microcontroller board (Arduino Uno) was used to connect the high-speed camera (Phantom v9.1, Vision Research) and the computer which ran a Matlab script to synchronize the ROT generator and video recording of cell electrorotation at a frame rate of 100 fps. The camera was mounted to a microscope (Axio Scope.A1, Carl Zeiss Microscopy) with a 50X dry objective. For each electrical excitation frequency, the acquired sequence of the 14-bit images was processed to determine the rotational speed of the microalgae cell. First, binarization was applied to convert grayscale images to binary images so that the microalgae cell could be identified. Noise was reduced by the threshold filtering. Microalgal cell projection in one of XY axis varies sinusoidally with time when the cell rotation is induced. Therefore, the rotational speed of the cell could be determined by sampling this time-varying signal with the Fast Fourier Transform. The uncertainty in the measurement of the rotational speed using this method was less than 3 % and analyzing time took less than 5 minutes for the whole spectrum of the cell (Lin et al. 2017).

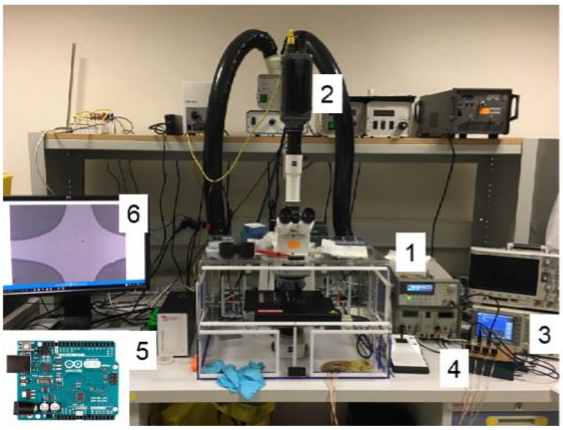

1	DEP generator
2	Fast camera
3	ROT generator
4	Electronic board
5	Arduino board
6	Computer

Figure 2. The electronic system for conducting electrorotation of single microal gae cells.

2.6 Double-shell ellipsoidal model and theoretical modeling

S. abundans is an ellipsoidal microalgae strain (length-to-width ratio of 1.1 6) with complex cell contents such as cell wall, cell membrane, cytoplasm, lipid d roplets, and starch grains. This study used a double-shell ellipsoidal model to re present the microalgal cells. The double-shell ellipsoidal model considered a *S. a bundans* cell as an ellipsoid with an inner core (cytoplasm, lipid droplets, etc.) enclosed by two outer shells (cell wall and cell membrane). The effective complex permittivity of the microalgal cell $\left(\underline{\varepsilon}^*_{cell\_\alpha}\right)$ in the double-shell ellipsoidal model along the $\alpha(\alpha = x, y)$ axis can be expressed as (Kakutani, Shibatani, and Sugai 199 3):

$$\underline{\varepsilon}^*_{cell\_\alpha} = \varepsilon^*_W \frac{\varepsilon^*_W + \left(\underline{\varepsilon}^*_{2\alpha} - \varepsilon^*_W\right)\left[A_{1\alpha} + v_1\left(1 - A_{0\alpha}\right)\right]}{\varepsilon^*_W + \left(\underline{\varepsilon}^*_{2\alpha} - \varepsilon^*_W\right)\left(A_{1\alpha} - v_1 A_{0\alpha}\right)} \qquad \alpha = x, y \tag{2}$$

$$\underline{\varepsilon}^*_{2\alpha} = \varepsilon^*_M \frac{\varepsilon^*_M + (\varepsilon^*_I - \varepsilon^*_M)\left[A_{2\alpha} + v_2\left(1 - A_{1\alpha}\right)\right]}{\varepsilon^*_W + (\varepsilon^*_I - \varepsilon^*_M)\left(A_{2\alpha} - v_2 A_{1\alpha}\right)} \qquad \alpha = x, y \tag{3}$$

$$\varepsilon^*_k = \varepsilon_k - j\frac{\sigma_k}{w} \tag{4}$$

$$v_1 = \frac{a_1 b_1 c_1}{a_0 b_0 c_0} \tag{5}$$

$$v_2 = \frac{a_2 b_2 c_2}{a_1 b_1 c_1} \tag{6}$$

$$a_1 = a_0 - wt, \quad b_1 = b_0 - wt, \quad c_1 = c_0 - wt \tag{7}$$

$$a_2 = a_1 - mt, \quad b_2 = b_1 - mt, \quad c_2 = c_1 - mt \tag{8}$$

$$A_{ix} = 0.5 a_i b_i c_i \int_0^\infty \frac{d\xi}{\left(a_i^2 + \xi\right) R_i} \qquad i = 0, 1, 2 \tag{9}$$

$$A_{iy} = 0.5 a_i b_i c_i \int_0^\infty \frac{d\xi}{\left(b_i^2 + \xi\right) R_i} \qquad i = 0, 1, 2 \tag{10}$$

$$R_i = \left[\left(a_i^2 + \xi\right)\left(b_i^2 + \xi\right)\left(c_i^2 + \xi\right)\right]^{1/2} \qquad i = 0,1 \tag{11}$$

where ε_W^*, ε_M^* and ε_I^* respectively stand for the complex permittivities of the cell wall, membrane and the inner core. The complex permittivity ε_k^* is dependent on the permittivity and conductivity ε_k and σ_k (k stands for W, M or I). a_0 is the major semi-axis of the cell and b_0, c_0 are the minor semi-axis of the cell. wt, mt are the thickness of the cell wall and the cell membrane. A_{ix} and A_{iy} are the depolarizing factors along the x, y axes respectively. ξ is the parameter used to represent a family of the surface of confocal ellipsoids. w represents the angular frequency of the electric field and $j^2 = -1$.

During electrorotation experiments, the rotational speed $\Omega_{cell}(w)$ of a cell is:

$$\Omega_{cell}(w) = \left(0.5E^2/R_f\right)\{Im[\mu_x(\omega) + \mu_y(\omega)]\} \tag{12}$$

$$\mu_\alpha(\omega) = V_c\varepsilon_0\frac{\varepsilon_{cell\_\alpha}^* - \varepsilon_{medium}^*}{\left(\varepsilon_{cell\_\alpha}^* - \varepsilon_{medium}^*\right)A_{0\alpha} + \varepsilon_{medium}^*} \qquad \alpha = x,y \tag{13}$$

$$V_c = \frac{4\pi a_0 b_0 c_0}{3} \tag{14}$$

$$R_f = 2V_c\eta\left[\left(a_0^2 + b_0^2\right)/\left(a_0^2 A_{0x} + b_0^2 A_{0y}\right)\right] \tag{15}$$

where η is the dynamic viscosity of the medium, E is the electric field at the center of the microelectrode set, ε_0 is the vacuum permittivity, ε_{medium}^* is the complex permittivity of the medium. $Im[\mu_x(\omega) + \mu_y(\omega)]$ is the imaginary part of the sum of the polarizability of the double-shell ellipsoid along the x and y axis.

The theoretical simulation of electrorotation of *S. abundans* single cells was conducted using the double-shell ellipsoidal model. The mechanical rotation speed of a cell is calculated by eq(12). The relative permittivity of cell wall, membrane, cytoplasm and lipid were set as 75, 8, 50, 4, respectively. The conductivity of cell wall, membrane, cytoplasm and lipid were set as 0.1 S/m, 2×10^{-5} S/m, 0.15 S/m, and 1×10^{-12} S/m (Müller, Schnelle, and Fuhr 1998). Other parameters used in the calculation were listed in table 1. To understand the effects of lipids on the electrorotation, the volume fraction of lipid was changed from 10 % (v/v) to 40 % (v/v) with an interval of 5 % (v/v), while a constant thickness of cell wall of 30 nm was used. On the other hand, to elucidate the effects of cell wall thickness, the thickness of the cell wall varied from 30 nm to 210 nm with an interval of 30 nm while a constant lipid fraction of 10 % (v/v) was applied. The complex dielectric properties of the inner core, which contained cytoplasm and lipid, were approximated by the mixing theory:

$$\varepsilon_I^* = \varepsilon_{cytoplasm}^* \frac{1 + 2\delta_{lipid} \frac{\varepsilon_{lipid}^* - \varepsilon_{cytoplasm}^*}{\varepsilon_{lipid}^* + 2\varepsilon_{cytoplasm}^*}}{1 - \delta_{lipid} \frac{\varepsilon_{lipid}^* - \varepsilon_{cytoplasm}^*}{\varepsilon_{lipid}^* + 2\varepsilon_{cytoplasm}^*}} \quad (16)$$

where ε_{lipid}^* is the complex permittivity of lipid, $\varepsilon_{cytoplasm}^*$ is the complex permittivity of cytoplasm.

Table 1. Parameters used in the fitting of the electrorotation spectra.

Parameter	Value	Unit
Vacuum permittivity (ε_0)	8.85×10^{-12}	F/m
Relative permittivity of medium (ε_{medium})	8×10^{1}	
Conductivity of medium (σ_{medium})	1.2×10^{-1}	S/m
Thickness of membrane (mt)	5×10^{-9}	m
Electric field (E)	2.0×10^{4}	V/m
Viscosity of medium (η)	1×10^{-3}	kg/(s·m)

2.7 Fitting of experimental electrorotation spectra

Two cases were applied to fit the experimental data to obtain the dielectric parameters (conductivity and permittivity) of microalgae based on the double-shell ellipsoidal model. The first case took account of thickening cell wall and the thickness of the cell wall (wt) in eq(7) increased when the duration of nitrogen starvation increased. The cell wall thickness was determined by TEM pictures as 30 nm for day 0 and 150 nm for day 7. The outer shell thicknesses for other time points were determined by assuming a linear increment, which estimated the outer shell thickness of 70 nm for day 3 and 110 nm for day 5. The second case considered constant cell wall thickness and the thickness of the cell wall in eq(7) was set as 30 nm.

To fit the experimental electrorotation spectra to these cases, the genetic algorithm (GA) in MATLAB software (MathWorks, Natick, MA) was employed. The searching boundaries of the dielectric properties and parameters listed in table 2 were set according to the information obtained in previous studies (Wang et al. 1997; Müller, Schnelle, and Fuhr 1998; Y. Wu et al. 2005; Han, Huang, and Han 2019). The size of cells with different lipid contents applied in the model was the average value measured from ten *S. abundans* cells. The GA algorithm randomly changed the value of dielectric parameters and adjusted these values by using mutation to minimize the difference between experimental results and models. The objective function needed to be minimized in this study is:

$$f(w,p) = \sum \quad \|z - \Omega(w,p)\|^2 \tag{17}$$

where z is the measured rotational velocity of the cell, $\Omega(w,p)$ is the rotational velocity obtained from the model, p is a vector composed of the estimated parameters (the conductivities and permittivities of inner compartment and shell).

A simplified inner core containing the mixture of water and lipid were then applied to approximate the total cellular lipids by the obtained dielectric properties with the general mixing formula (Uvarov 2000) and the Maxwell Garnett equation:

$$\sigma_I = (1 - \delta_{lipid})\sigma_{water} + \delta_{lipid}\sigma_{lipid} \tag{18}$$

$$\varepsilon_I = \varepsilon_{water} \frac{\varepsilon_{lipid} + 2\varepsilon_{water} + 2\delta_{ipid}(\varepsilon_{lipid} - \varepsilon_{water})}{\varepsilon_{lipid} + 2\varepsilon_{water} - \delta_{ipid}(\varepsilon_{lipid} - \varepsilon_{water})} \tag{19}$$

where σ_{water}, σ_{lipid} is the conductivity of water and lipid and set as 0.15 S/m and 1×10^{-12} S/m, ε_{water}, ε_{lipid} is the relative permittivity of water and lipid and set as 80 and 4, and δ_{lipid} is the volume fraction of the lipid (Lizhi, Toyoda, and Ihara 2008).

Table 2. Upper and lower limits of the dielectric parameters set in the genetic algorithm.

Parameters	Lower bound	Higher bound
Relative permittivity of inner core (ε_I)	4×10^{1}	7×10^{1}
Conductivity of inner core (σ_I)	1×10^{-2}	1×10^{1}
Relative permittivity of membrane (ε_M)	1×10^{0}	8×10^{1}
Conductivity of membrane (σ_M)	1×10^{-6}	1×10^{-2}
Relative permittivity of cell wall (ε_W)	1×10^{0}	8×10^{1}
Conductivity of cell wall (σ_M)	1×10^{-6}	1×10^{-2}

3. Results and Discussions

3.1 Effects of nitrogen starvation on S. abundans

Nitrogen starvation induced apparent lipid accumulation inside *S. abundans* cells but insignificant change in cell sizes. At day 0 (beginning of nitrogen starvation), *S. abundans* had a total lipid content of 15.3 wt%. The total lipid content increased to around 21 wt% after 3 days and further increased to 33.8 wt% on the 7th day, which agreed with the values found in previous reports (Valdez-Ojeda et al. 2015; Rai and Gupta 2017). Since the rotational velocity is size dependent, cell size was also investigated and shown in figure 3. The major axis and minor axis of

elliptical *S. abundans* cells were determined by ImageJ™. At day 0, the average major and minor axis of *S. abundance* cells was 4.4 μm ± 0.3 μm and 3.9 ± 0.3 μm, respectively. The cell size remained similar within 5 days, and then increased slightly to 4.9 μm ± 0.1 μm and 4.2 ± 0.1 μm, which corresponded to a 7 % of variation, after the 7-day nitrogen starvation.

In addition to lipid accumulation, nitrogen starvation induced considerable cell wall thickening for *S. abundans*. The transmission electron microscope (TEM) images (figure 7) showed that *S. abundans* contained a high volumetric fraction of lobe-shaped chloroplasts in the cytoplasm before nitrogen starvation. However, the volume of storage subcompartments such as lipid droplets and starch grains in the cytoplasm increased considerably after 7 days of nitrogen starvation. In addition, the average cell wall thickness increased from 30 nm to 150 nm although the cell size did not increase significantly after nitrogen starvation. The thickening of cell wall was also reported and has been considered a protective mechanism for cells under environmental stresses (Bohnert, Nelson, and Jensen 1995; Van Donk et al. 1997). For example, *Chlamydomonas reinhardtii* thickened their cell wall by around 8-fold when experienced nitrogen depletion (Bensalem et al. 2018). The composition of thickened cell wall was mainly carbohydrates produced through the fixation of carbon dioxide for several microalgae strains such as *Neochloris oleoabundans*, *Desmodesmus sp.*, and *Nannochloropsis salina (Baulina et al. 2016; Jeong et al. 2017; Rashidi et al. 2019)*. *Desmodesmus sp.* thickened its cell wall by 30 % to 160 % under nitrogen depletion and the polysaccharide layer contributed to a greater part of the thickened cell wall compared with the sporopollenin layer. As for the structure of outer cell wall, net-like structures and chimney-like rosettes can both be observed in TEM images before and after nitrogen starvation. This agrees with the observation in a previous study (Hegewald and Schnepf 1991) and suggests that nitrogen starvation had little effects on the surface of outer cell wall of *S. abundans*.

The electrorotation spectra of *S. abundans* cells was altered by multiple cellular changes during the nitrogen starvation. The maximal rotation velocity decreased while the lipid content increased from 15.3 wt% to 21.1 wt%, then remained comparable when the total lipid content increased to 33.8 wt% as shown in figure 5a. This indicated that the amount of cellular lipids was not the only factor affecting the maximal rotational velocity. The reverse frequency is the frequency at which the imaginary part of the Clausius-Mossotti factor changes from negative to positive, corresponding to the change of cell rotation direction from against to along the applied electric field. The reverse frequency decreased from 25 MHz to 20 MHz while the total lipid content increased from 15.3 wt% to 33.8 wt% (figure 5b). These results are similar to previously published data. The reverse frequency of heterotrophic *Chlorella protothecoides* was lower than the one of autotrophic culture and this had been related to the accumulation of lipids in the heterotrophic cells (Y. Wu et al. 2005). *Chlamydomonas reinhardtii* with a high lipid content also had a lower reverse frequency in the electrorotation spectra compared with those with a low lipid content (Han, Huang, and Han 2019). The correlation between the reverse frequency and total lipid contents suggested the possibility of using the change in dielectric properties to characterize the cytoplasmic contents.

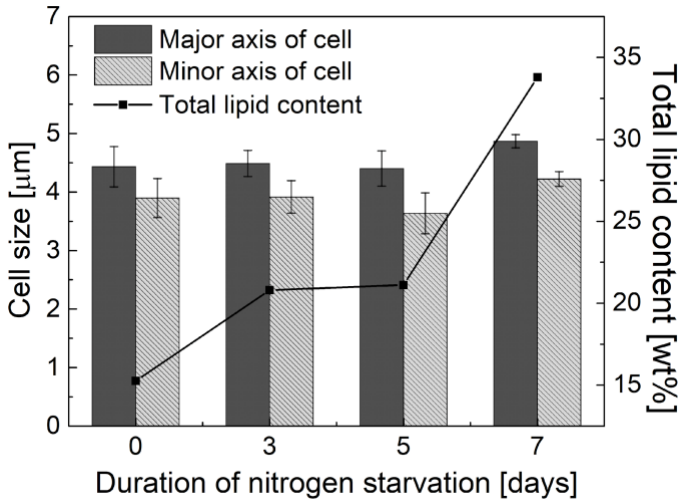

Figure 3. The change of total lipid contents and cell size in the nitrogen starvation period.

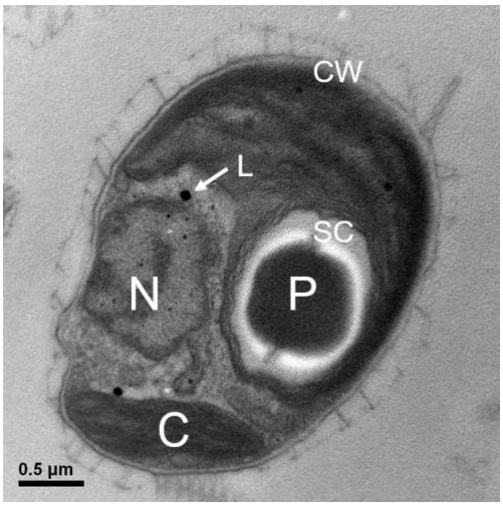

(a)

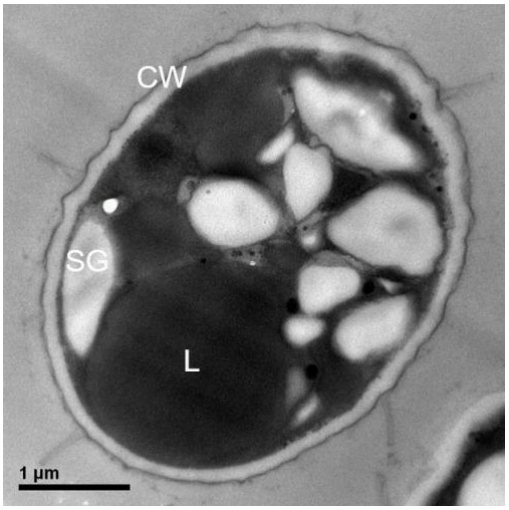

(b)

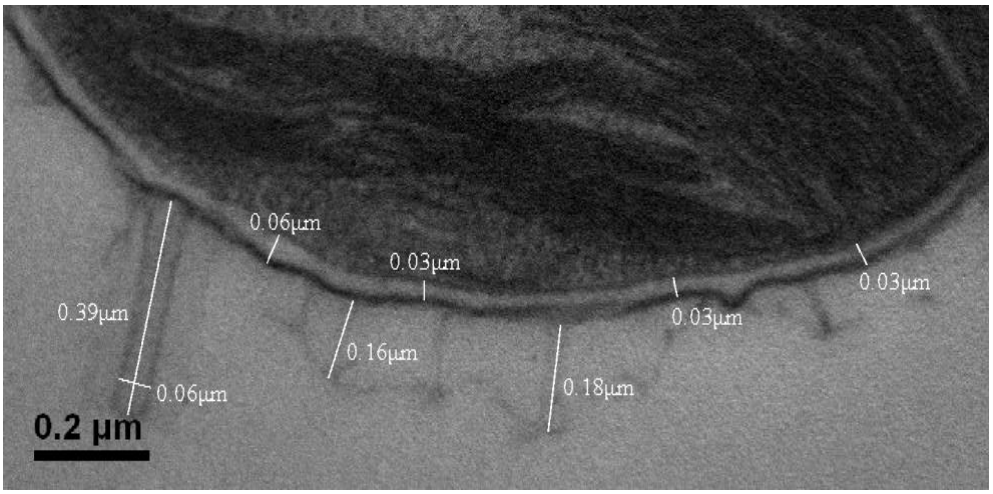

(c)

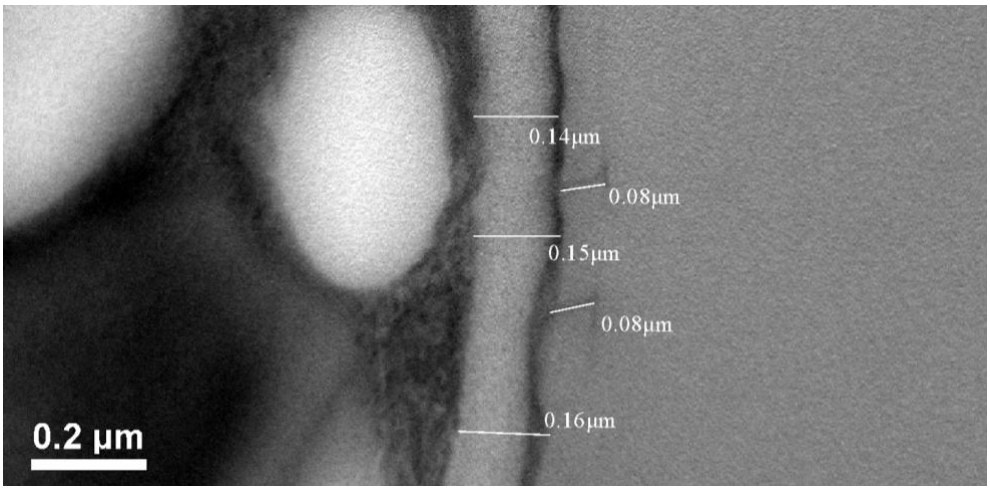

(d)

Figure 4. The transmission electron microscope (TEM) picture of *S. abundans* cells at different days of nitrogen starvation. (a) day 0; (b) day 7. The cell at day 0 had a high fraction of chloroplast while the cell at day 7 had a high fraction of lipid and starch. N, nucleus; C, chloroplast; P, pyrenoid; L, lipid; SC, starch capsule; CW, cell wall. The blowup of *S. abundans* cells at different days of nitrogen starvation. (c) day 0; (d) day 7. The thickness of cell wall at day 0 was around 30-40 nm while the thickness of cell wall at day 7 was around 140-160 nm.

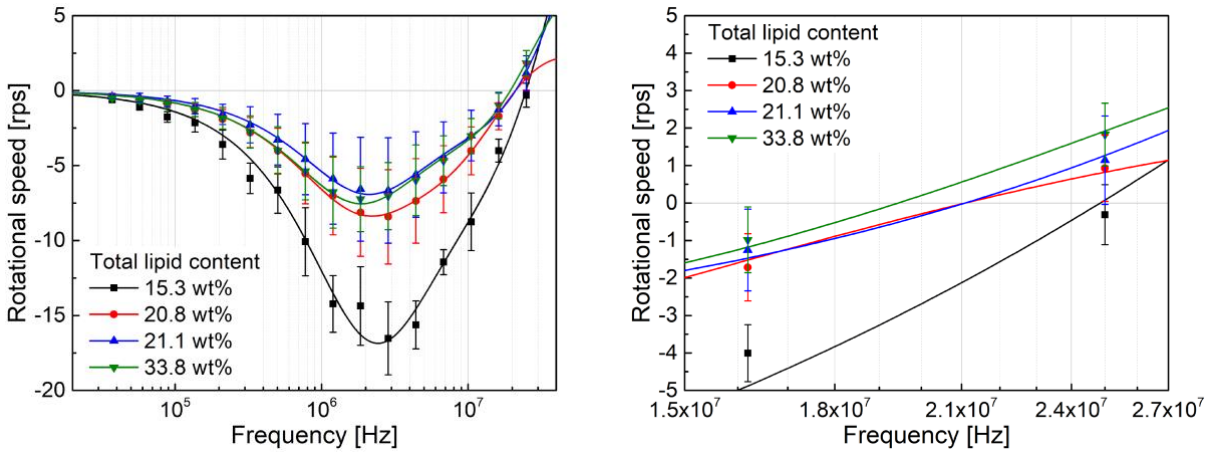

(a) (b)

Figure 5. The electrorotation spectra of *S. abundans* cells with different total lipid contents. (a) the full spectra of cells; (b) the blowup between 1.5×10^7 Hz and 2.7×10^7 Hz to clearly show the reverse frequency.

3.2 Theoretical simulation of electrorotation spectra

The theoretical simulation of electrorotation spectra indicated that lipid accumulation and cell wall thickening have similar effects on the peak rotation velocity but dissimilar effects on other spectral characteristics. The effects of the total lipid content a on the electrorotation spectra and the cell wall thickness are shown in figure 6. The dielectric properties of inner core applied in the simulation were approximated by the mixing theory (eq(16)). Figure 6a shows that the volumetric fraction of lipids affected the electrorotation spectra when the frequency

was higher than 100 kHz. The reverse frequency decreased from 6.4 MHz to 5.1 MHz and the peak value of rotation velocity increased from -30.4 to -19.2 as the lipid fraction increased from 10 % (v/v) to 40 % (v/v). However, the increase of cellular lipids had little effects on the electrorotation spectra in the low frequency region. This is similar to the observation in (Michael, Hiibel, and Geiger 2014), which indicated that the dielectric properties of the cytoplasm dominated the dielectric behavior of the whole cell at high frequencies. The thickening cell wall had similar effects to the increasing lipid fraction on the peak value of rotation velocity. The thicker cell wall led to a 16 % increase in the peak value of rotation velocity while the higher lipid fraction led to a 37 % increase. However, the cell wall thickness started to affect the electrorotation spectra at a much lower frequency of 20 kHz (figure 6b) compared with the lipid fraction. Moreover, the thickening cell wall had little effect on the reverse frequency, contrary to the decrease of reverse frequency from 6.4 MHz to 5.1 MHz when the lipid fraction increased. Finally, the increase of total lipid fraction resulted in a shift in the peak frequency (the frequency where the rotation velocity was the highest), and this was not observed in the case of increasing cell wall thickness. Another interesting finding was a node at the frequency around 5 MHz, where the cell wall thickness had no effect on the electrorotation spectra, compared with a node at frequency around 9 MHz which the higher lipid fraction had no effect on the electrorotation spectra.

According to the simulations, changes of electrorotation spectra at low frequency regions can be the indicator for changing cell wall properties. For example, in figure 5, electrorotation spectra of cells with different total lipid contents started to show differences at frequency as low as 50 KHz and this indicated the parallel changes of cell wall thickness. The peak value of rotation velocity is decreased by either lipid accumulation or cell wall thickening; therefore, the decrease in the peak value alone cannot be a direct indicator of the cellular change. However, if the decrease of peak rotation velocity value was accompanied by a shifting peak frequency, cellular lipid accumulation can be expected. This also agreed with the experimental data shown in figure 5, which illustrated the decrease of peak rotation velocity by 60 % and the shift of peak frequency from 3 MHz to 2 MHz. Overall, the electrorotation spectra was susceptible to both cell wall thickness and lipid fraction as observed from the theoretical calculation. This shows that, as the frequency increased to a certain value, the interfacial relaxation resonance occurred simultaneously in cell wall, cell membrane, cytoplasm, and lipids. Therefore, fitting the experimental data to the double-shell model considering the thickening cell wall is critical to accurately extract the cellular dielectric properties.

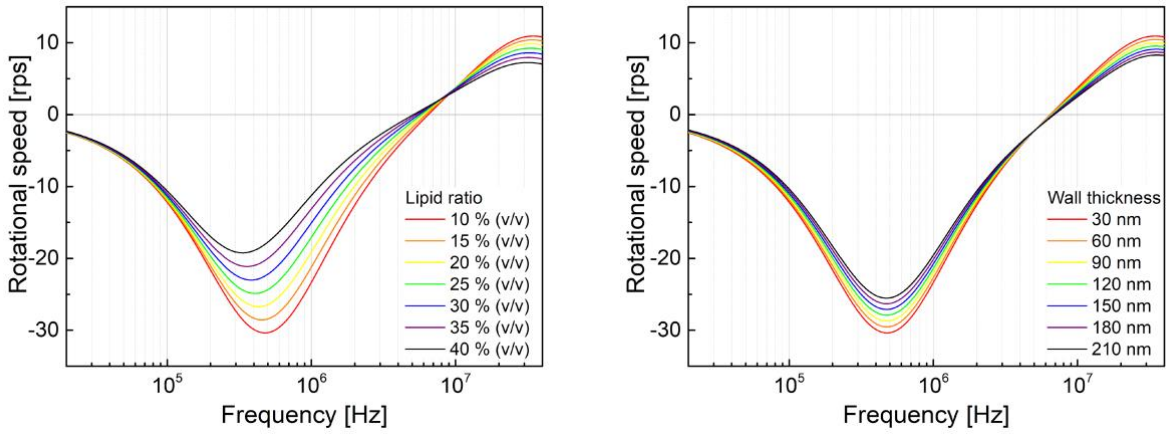

(a) (b)

Figure 6. The calculated imaginary part of the Clausius-Mossotti factor when (a) the lipid fraction changed from 10 % (v/v) to 40 % (v/v) with a constant cell wall thickness of 30 nm and (b) the cell wall thickness changed from 30 nm to 210 nm with a constant lipid ratio of 10 % (v/v).

3.3 Fitting of experimental data with double-shell ellipsoidal model considering thickening cell wall

The accurate interpretation of electrorotation spectra was achieved with the inclusion of a thickening cell wall in the double-shell ellipsoidal model. Figure 9 a shows the good agreements between experimental data and model predictions for *S. abundans* cells when applying the double-shell ellipsoidal model and taking the thickening cell wall into account. The obtained dielectric parameters for *S. abundans* cells with different total lipid contents are listed in table 3. The conductivity (σ_M) and relative permittivity (ε_M) of membrane increased from 4.5×10^{-4} S/m to 6.05×10^{-3} S/m and from 3.03 to 7.83, respectively, when the total lipid content increased from 15.3 wt% to 33.8 wt%. Cell membrane had slightly increased its relative permittivity which agreed with a 3-fold increase in the specific capacitance of membrane observed in the heterotrophic cells (Y. Wu et al. 2005). The conductivity (σ_W) and relative permittivity (ε_W) of the cell wall increased from 7.02×10^{-4} S/m to 8.19×10^{-3} S/m and from 13.79 to 49.87, respectively, when the total lipid content increased from 15.3 wt% to 33.8 wt%. These results showed that the cell wall was more influential than cell membrane on electrorotation spectra under these cultural conditions. Polysaccharides were the main composition of the thickened cell wall during nitrogen starvation and polysaccharides containing conjugated forms had a wide range and high values of permittivity (Pohl 1986; Mohammady 2004). Therefore, the greatly increased ε_W for *S. abundans* can be explained by the 5-fold increase in cell wall thickness observed in the TEM images as shown in figure 7. Similar phenomena of elevated permittivity due to accumulation of polysaccharides were also reported in bacterial biofilm studies. The buildup of extracellular polymeric substance (EPS), which contains a large amount of polysaccharides, increased the capacitance of biofilm substantially (Singh 2014). The increased σ_W and ε_W were consistent with the results obtained in (Y. Wu et al. 2005), which applied a three-shell model to study the difference in dielectric properties between heterotrophic (high-lipid) and autotrophic (low-lipid) *Chlorella protothecoides* cells. A 4-fold in

crease in the conductivity and an 8-fold increase in the specific capacitance of cell wall were found in the heterotrophic cells and this was attributed to the rougher and larger surface area of the cell wall on these high-lipid cells (Y. Wu et al. 2005). Analysis of cell wall composition under stress such as nitrogen starvation drew increasing attention in recent years (Baulina et al. 2016; Rashidi and Trindade 2018; Rashidi et al. 2019). Nevertheless, the effect of altered cell wall properties, due to stresses, on electrorotation spectra have never been considered until this study. Thick microalgae cell walls of microalgae formed a firm barrier against the contact of organic solvents and cellular lipids during the extraction process. Moreover, the cell wall composition changed with the growth conditions and culture periods. In order to extract lipids effectively for commercial production of biodiesel, good understanding of the structure and characteristics of cell walls is necessary (Kim et al. 2016; Rashidi and Trindade 2018; Alhattab, Kermanshahi-Pour, and Brooks 2019). The electrorotation spectra provides timely and useful information in evaluating cell wall properties for facilitating lipid extraction.

Table 3. The dielectric parameters of *S. abundans* obtained from the double-shell ellipsoidal model considering thickening cell wall

Total lipid content (wt%)	ε_I	σ_I (S/m)	ε_M	σ_M (S/m)	ε_W	σ_W (S/m)
15.3	63.96	1.26×10^{-1}	3.03	4.5×10^{-4}	13.79	7.02×10^{-4}
20.8	59.73	1.18×10^{-1}	5.93	8.41×10^{-3}	39.15	5.65×10^{-3}
21.1	54.12	1.12×10^{-1}	6.65	8.43×10^{-3}	42.02	7.19×10^{-3}
33.8	49.59	9.87×10^{-2}	7.83	6.05×10^{-3}	49.87	8.19×10^{-3}

The dielectric properties of the inner core provided information for quantitative assessment of the total cellular lipid content. After nitrogen starvation, the conductivity of inner core (σ_I) decreased from 1.26×10^{-1} S/m to 9.87×10^{-2} S/m while the lipid content increased from 15.3 wt% to 33.8 wt%. Also, the relative permittivity of inner core (ε_I) gradually decreased from 63.96 to 49.59. Existing studies, with the consideration of thickening cell wall or not, only showed the difference of dielectric properties between low-lipid and high-lipid microalgae cells (Haddady et al. 2014; Lin et al. 2017; Han, Huang, and Han 2019) and lacked the quantitative assessment of total lipid contents. The results in this study provided the possibility of applying ε_I and $\sigma_I$to quantify the amount of lipids inside the *S. abundans* cells. The calculated lipid contents from ε_I and σ_I, using mixing formulas (eq(18) and eq(19)), were plotted against the measured lipid contents and a good agreement was achieved as shown in figure 8b. This is the first success in using the dielectric parameters obtained from electrorotation spectra to quantify the cell

ular lipid content and the error between predicted and measured values can be as low as 0.22 wt%. Among ε_I and σ_I, the latter more accurately quantified the total lipid contents with an average error of 1.13 wt%. The average error of total lipid contents estimated by ε_I was 2.23 wt%.

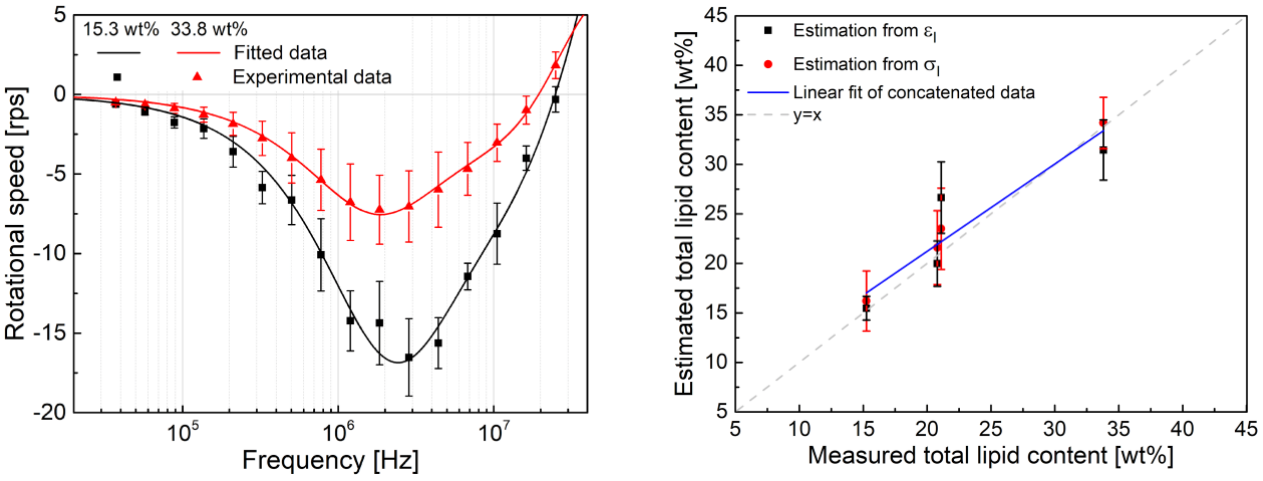

(a) (b)

Figure 9. (a) The fitting of experimental electrorotation spectra of *S. abundans* containing 15.3 wt% and 33.8 wt% of lipids by using the double-shell ellipsoidal model considering cell wall; (b) The relationship between measured total lipid contents and calculated lipid contents from permittivities (ε_I) and conductivities (σ_I) of inner core listed in table 3.

3.4 Fitting of experimental data with double-shell ellipsoidal model with constant cell wall thickness

Leaving the thickening cell wall out of the double-shell ellipsoidal model can lead to the misinterpretation of electrorotation spectra. The permittivity and conductivities of *S. abundans* cells obtained from the double-shell ellipsoidal model neglecting the thickening cell wall are listed in table 4. The conductivity of cell wall (σ_W), which had a fixed-thickness of 30 nm, was the most sensitive parameters and an increase from 1.1×10^{-3} S/m to 3.33×10^{-3} S/m was found as the total lipid content increased from 15.3 wt% to 33.8 wt%. Meanwhile, the permittivity of cell wall (ε_W) increased from 13.67 to 33.67. The conductivity (σ_M) and relative permittivity (ε_M) of the cell membrane increased from 3.86×10^{-4} S/m to 1.01×10^{-3} S/m and from 3.32 to 4.31, respectively. Even though there were good agreements between experimental data and model predictions for *S. abundans* cells as shown in figure 10. Although the increase of permittivity of cell membrane can be explained by the less insulated and looser cell membrane during nitrogen starvation as indicated in (Jeong et al. 2017), the barely changed conductivity (σ_I) and permittivity (ε_I) of the inner core disregarding the increasing total lipid contents is not in agreement with common expectations considering the low conductivity and permittivity of lipids. Furthermore, the total lipid contents approximated by the mixing formulas, eq(18) and eq(19), were not in agreement with the measured values (figure 10b). Such discrepancy in terms of dielectric properties showed the importance in taking the thickening cell wall into consideration to correctly interpret the electrorotation spectra. Nonetheless, existing studies did not address the thickening of cell w

all and were able to observe decreases in σ_I and ε_I when the microalgae accumulated lipids in the cytoplasm (Hadady et al. 2014; Han, Huang, and Han 2019). In (Hadady et al. 2014), the cytoplasmic conductivity was deduced from upper crossover frequency of dielectrophoresis and a decrease from 0.2267 S/m to 0.095 S/m was found when the lipid content increased. The contribution of the outer shell became negligible at such high frequencies, making the dielectric measurement insensitive to the cell wall thickness. However, dielectric measurements at high frequencies are highly demanding in instruments and not practical for commercial applications. In (Han, Huang, and Han 2019), similar cell wall thickness between *Chlamydomonas reinhardtii* cells before and after nitrogen starvation was observed from the microscopic images. Therefore, using constant cell wall thickness in their study still produced reasonable outcomes. The cytoplasmic conductivity derived from the electrorotation spectrum of *Chlamydomonas reinhardtii* with low and high lipid contents were 0.38 S/m and 0.22 S/m, respectively. The same study also reported the decrease of relative permittivity of inner core from 130 to 76 when the lipid contents increased. However, cell wall thickening is commonly observed in stressed microalgae cells and occurs simultaneously with lipid accumulation. It is necessary to include cell wall thickening in the dielectric model to accurately interpret electrorotation spectra of microalgae cells under stresses in future studies.

Table 4. The dielectric parameters of *S. abundans* obtained from the double-shell ellipsoidal model with constant cell wall thickness (30 nm).

Total lipid content (wt%)	ε_I	σ_I (S/m)	ε_M	σ_M (S/m)	ε_W	σ_W (S/m)
15.3	65.48	1.25×10^{-1}	3.32	3.86×10^{-4}	13.67	1.10×10^{-3}
20.8	64.61	1.25×10^{-1}	3.98	9.09×10^{-4}	21.52	2.96×10^{-3}
21.1	63.50	1.23×10^{-1}	3.95	1.04×10^{-3}	26.75	3.27×10^{-3}
33.8	65.11	1.26×10^{-1}	4.31	1.01×10^{-3}	33.67	3.33×10^{-3}

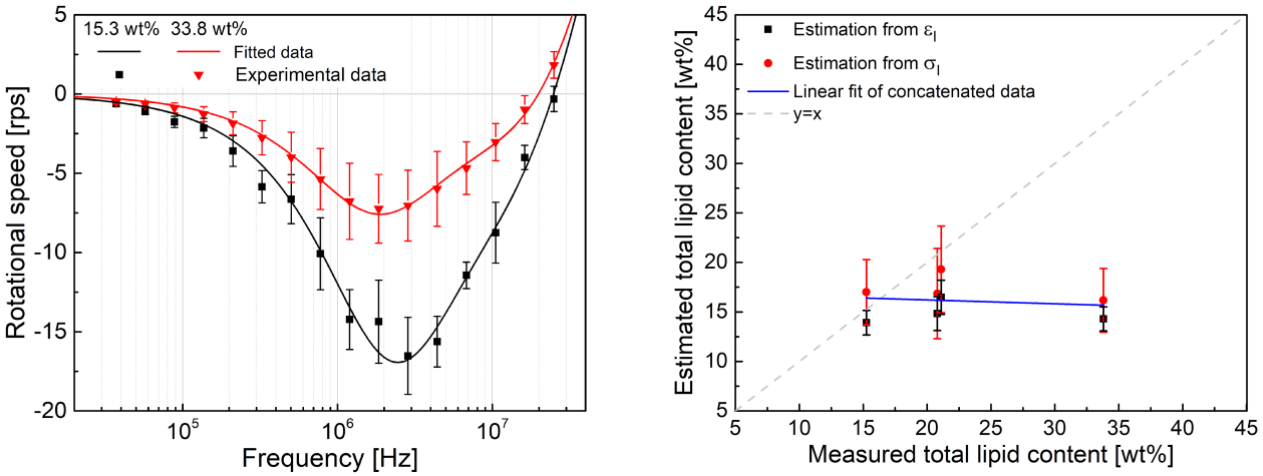

(a) (b)

Figure 10. (a) The fitting of experimental electrorotation spectra of *S. abundans* containing 15.3 wt% and 33.8 wt% of lipids by using the double-shell ellipsoidal model with constant cell wall thickness; (b) The relationship between measured total lipid contents and calculated lipid contents from permittivities (ε_I) and conductivities (σ_I) of inner core shown in table 4.

4. Conclusions

This study demonstrated the use of electrorotation to characterize the dielectric properties of single microalgal cells and the estimation of the total cellular lipid content from these dielectric properties. The theoretical and experimental electrorotation spectra of *Scenedesmus abundans* cells were studied during nitrogen starvation and the results showed that both total cellular lipid contents and cell wall properties have considerable effects on the electrorotation spectra. The double-shell ellipsoidal model considering thickening cell wall was applied to deduce the dielectric properties of outer shell and inner core from electrorotation spectra. When the total cellular lipid content increased from 15.3 wt% to 33.8 wt%, the conductivity and relative permittivity of the inner core (a mixture of cytoplasm, lipid droplets, and nucleus) decreased by 21.7 % and 22.5 %, respectively. These dielectric properties were then applied to estimate total lipid contents by using the mixing formula and a good agreement was found between the estimated and measured values with the error as less as 0.22 wt%. The structural and compositional changes of cell wall during nitrogen starvation were also revealed by the increases in the conductivity and relative permittivity of the cell wall. To our best knowledge, this is the first study that succeeds in applying electrorotation on quantifying total cellular lipids of microalgae cells.

Acknowledgements

This study is supported by the Ministry of Science and Technology of Taiwan under grant number MOST 105-2911-I-007-525, MOST 105-2221-E-002-112-MY3, and LABEX Lasips (ANR-10-LABX-0040-LaSIPS) managed by the French National Research Agency under the "Investissements d'avenir" program (n° ANR-11-IDEX-0003-02).

The authors are grateful to the staff of the Technology Commons in the College of Life Science at National Taiwan University for their assistance with transmission electron microscopy. Appreciation also goes to the Data Analysis and Interpreta

tion Lab in the Department of Engineering and System Science of National Tsing Hua University, Taiwan for the assistance in fitting algorithms.

Reference

Alhattab, Mariam, Azadeh Kermanshahi-Pour, and Marianne Su-Ling Brooks. 2019. “Microalgae Disruption Techniques for Product Recovery: Influence of Cell Wall Composition.” *Journal of Applied Phycology* 31 (1): 61-88.

Axelsson, Martin, and Francesco Gentili. 2014. “A Single-Step Method for Rapid Extraction of Total Lipids from Green Microalgae.” *PloS One* 9 (2): e89643.

Baulina, Olga, Olga Gorelova, Alexei Solovchenko, Olga Chivkunova, Larisa Semenova, Irina Selyakh, Pavel Scherbakov, Olga Burakova, and Elena Lobakova. 2016. “Diversity of the Nitrogen Starvation Responses in subarcticDesmodesmussp. (Chlorophyceae) Strains Isolated from Symbioses with Invertebrates.” *FEMS Microbiology Ecology*. https://doi.org/10.1093/femsec/fiw031.

Bensalem, Sakina, Filipa Lopes, Pierre Bodénès, Dominique Pareau, Olivier Français, and Bruno Le Pioufle. 2018. “Understanding the Mechanisms of Lipid Extraction from Microalga Chlamydomonas Reinhardtii after Electrical Field Solicitations and Mechanical Stress within a Microfluidic Device.” *Bioresource Technology* 257 (June): 129-36.

Bohnert, H. J., D. E. Nelson, and R. G. Jensen. 1995. “Adaptations to Environmental Stresses.” *The Plant Cell*. https://doi.org/10.1105/tpc.7.7.1099.

Breuer, Guido, Packo P. Lamers, Dirk E. Martens, René B. Draaisma, and René H. Wijffels. 2013. “Effect of Light Intensity, pH, and Temperature on Triacylglycerol (TAG) Accumulation Induced by Nitrogen Starvation in Scenedesmus Obliquus.” *Bioresource Technology* 143 (September): 1-9.

Chen, Bailing, Chun Wan, Muhammad Aamer Mehmood, Jo-Shu Chang, Fengwu Bai, and Xinqing Zhao. 2017. “Manipulating Environmental Stresses and Stress Tolerance of Microalgae for Enhanced Production of Lipids and Value-Added products-A Review.” *Bioresource Technology* 244 (November): 1198-1206.

Dean, Andrew P., David C. Sigee, Beatriz Estrada, and Jon K. Pittman. 2010. “Using FTIR Spectroscopy for Rapid Determination of Lipid Accumulation in Response to Nitrogen Limitation in Freshwater Microalgae.” *Bioresource Technology* 101 (12): 4499-4507.

Deng, Yu-Luen, Mei-Yi Kuo, and Yi-Je Juang. 2014. “Development of Flow through Dielectrophoresis Microfluidic Chips for Biofuel Production: Sorting and Detection of Microalgae with Different Lipid Contents.” *Biomicrofluidics* 8 (6): 064120.

Français, Olivier, and Bruno Le Pioufle. 2017. “Single Cell Electrical Characterization Techniques.” https://doi.org/10.1007/978-3-319-26779-1_15-1.

Hadady, Hanieh, Doug Redelman, Sage R. Hiibel, and Emil J. Geiger. 2016. “Continuous-Flow Sorting of Microalgae Cells Based on Lipid Content by High Frequency Dielectrophoresis.” *AIMS Biophys* 3: 398-414.

Hadady, Hanieh, Johnson J. Wong, Sage R. Hiibel, Doug Redelman, and Emil J. Geiger. 2014. “High Frequency Dielectrophoretic Response of Microalgae over Time.” *Electrophoresis* 35 (24): 3533-40.

Han, Song-I, Can Huang, and Arum Han. 2019. “Measurement of Dielectric Properties of Microalgae with Different Lipid Content Using Electrorotation and Negative Dielectrophoresis Cell Trap.” *2019 20th International Conference on Solid-Sta*

te Sensors, Actuators and Microsystems & Eurosensors XXXIII (TRANSDUCERS & EUROSENSORS XXXIII). https://doi.org/10.1109/transducers.2019.8808499.

Hegewald, E., and E. Schnepf. 1991. "Scenedesmus Abundans (Kirchn.) Chod., an Older Name for Chlorella fuscaShih. et Krauss." *Archiv Für Protistenkunde*. https://doi.org/10.1016/s0003-9365(11)80015-1.

Huang, Liang, Fei Liang, Yongxiang Feng, Peng Zhao, and Wenhui Wang. 2020. "On-Chip Integrated Optical Stretching and Electrorotation Enabling Single-Cell Biophysical Analysis." *Microsystems & Nanoengineering* 6 (1): 57.

Jeong, Seok Won, Seung Won Nam, Kwon HwangBo, Won Joong Jeong, Byeong-Ryool Jeong, Yong Keun Chang, and Youn-Il Park. 2017. "Transcriptional Regulation of Cellulose Biosynthesis during the Early Phase of Nitrogen Deprivation in Nannochloropsis Salina." *Scientific Reports* 7 (1): 5264.

Johnson, J. M., and V. Rahmat-Samii. 1997. "Genetic Algorithms in Engineering Electromagnetics." *IEEE Antennas and Propagation Magazine*. https://doi.org/10.1109/74.632992.

Kakutani, Tadaaki, Shigeo Shibatani, and Makoto Sugai. 1993. "Electrorotation of Non-Spherical Cells: Theory for Ellipsoidal Cells with an Arbitrary Number of Shells." *Bioelectrochemistry and Bioenergetics* 31 (2): 131-45.

Kawai, Shikiho, Masato Suzuki, Satoshi Arimoto, Tsuguhiro Korenaga, and Tomoyuki Yasukawa. 2020. "Determination of Membrane Capacitance and Cytoplasm Conductivity by Simultaneous Electrorotation." *The Analyst* 145 (12): 4188-95.

Kim, Dong-Yeon, Durairaj Vijayan, Ramasamy Praveenkumar, Jong-In Han, Kyubock Lee, Ji-Yeon Park, Won-Seok Chang, Jin-Suk Lee, and You-Kwan Oh. 2016. "Cell-Wall Disruption and Lipid/astaxanthin Extraction from Microalgae: Chlorella and Haematococcus." *Bioresource Technology*. https://doi.org/10.1016/j.biortech.2015.08.107.

Lee, T. H., J. S. Chang, and H. Y. Wang. 2013. "Current Developments in High‐throughput Analysis for Microalgae Cellular Contents." *Biotechnology Journal*. https://onlinelibrary.wiley.com/doi/abs/10.1002/biot.201200391.

Lee, Tsung-Hua, Jo-Shu Chang, and Hsiang-Yu Wang. 2013. "Rapid and in Vivo Quantification of Cellular Lipids in Chlorella Vulgaris Using Near-Infrared Raman Spectrometry." *Analytical Chemistry*. https://doi.org/10.1021/ac3028118.

Lin, Yu-Sheng, Sung Tsang, Rasta Ghasemi, Sakina Bensalem, Olivier Français, Filipa Lopes, Hsiang-Yu Wang, Chen-Li Sun, and Bruno Le Pioufle. 2017. "Dielectric Characterisation of Single Microalgae Cell Using Electrorotation Measurements." *Proceedings*. https://doi.org/10.3390/proceedings1040543.

Li, Yan, Forough Ghasemi Naghdi, Sourabh Garg, Tania Catalina Adarme-Vega, Kristofer J. Thurecht, Wael Abdul Ghafor, Simon Tannock, and Peer M. Schenk. 2014. "A Comparative Study: The Impact of Different Lipid Extraction Methods on Current Microalgal Lipid Research." *Microbial Cell Factories* 13 (January): 14.

Lizhi, Hu, K. Toyoda, and I. Ihara. 2008. "Dielectric Properties of Edible Oils and Fatty Acids as a Function of Frequency, Temperature, Moisture and Composition." *Journal of Food Engineering* 88 (2): 151-58.

Mandotra, S. K., Pankaj Kumar, M. R. Suseela, and P. W. Ramteke. 2014. "Fresh Water Green Microalga Scenedesmus Abundans: A Potential Feedstock for High Quality Biodiesel Production." *Bioresource Technology* 156 (March): 42-47.

Martínez-Bisbal, M. Carmen, Noèlia Carbó Mestre, Ramón Martínez-Máñez, Jorge Bauzá, and Miguel Alcañiz Fillol. 2019. "Microalgae Degradation Follow up by Volt

ammetric Electronic Tongue, Impedance Spectroscopy and NMR Spectroscopy." *Sensors and Actuators. B, Chemical* 281 (February): 44-52.

Mata, Teresa M., António A. Martins, and Nidia S. Caetano. 2010. "Microalgae for Biodiesel Production and Other Applications: A Review." *Renewable and Sustainable Energy Reviews* 14 (1): 217-32.

Medipally, Srikanth Reddy, Fatimah Md Yusoff, Sanjoy Banerjee, and M. Shariff. 2015. "Microalgae as Sustainable Renewable Energy Feedstock for Biofuel Production." *BioMed Research International* 2015 (March): 519513.

Michael, Kelsey A., Sage R. Hiibel, and Emil J. Geiger. 2014. "Dependence of the Dielectrophoretic Upper Crossover Frequency on the Lipid Content of Microalgal Cells." *Algal Research*. https://doi.org/10.1016/j.algal.2014.08.004.

Mohammady, Nagwa Gamal. 2004. "Total, Free and Conjugated Sterolic Forms in Three Microalgae Used in Mariculture." *Zeitschrift Für Naturforschung C*. https://doi.org/10.1515/znc-2004-9-1002.

Müller, T., T. Schnelle, and G. Fuhr. 1998. "Dielectric Single Cell Spectra in Snow Algae." *Polar Biology*. https://doi.org/10.1007/s003000050307.

Patel, Alok, Io Antonopoulou, Josefine Enman, Ulrika Rova, Paul Christakopoulos, and Leonidas Matsakas. 2019. "Lipids Detection and Quantification in Oleaginous Microorganisms: An Overview of the Current State of the Art." *BMC Chemical Engineering* 1 (1): 13.

Pohl, Herbert A. 1986. "Giant Polarization in High Polymers." *Journal of Electronic Materials* 15 (4): 201-3.

Rai, Monika Prakash, and Shivani Gupta. 2017. "Effect of Media Composition and Light Supply on Biomass, Lipid Content and FAME Profile for Quality Biofuel Production from Scenedesmus Abundans." *Energy Conversion & Management* 141 (June): 85-92.

Rashidi, Behzad, Annemarie Dechesne, Maja G. Rydahl, Bodil Jørgensen, and Luisa M. Trindade. 2019. "Neochloris Oleoabundans Cell Walls Have an Altered Composition When Cultivated under Different Growing Conditions." *Algal Research*. https://doi.org/10.1016/j.algal.2019.101482.

Rashidi, Behzad, and Luisa M. Trindade. 2018. "Detailed Biochemical and Morphologic Characteristics of the Green Microalga Neochloris Oleoabundans Cell Wall." *Algal Research*. https://doi.org/10.1016/j.algal.2018.08.033.

Rumin, Judith, Hubert Bonnefond, Bruno Saint-Jean, Catherine Rouxel, Antoine Sciandra, Olivier Bernard, Jean-Paul Cadoret, and Gaël Bougaran. 2015. "The Use of Fluorescent Nile Red and BODIPY for Lipid Measurement in Microalgae." *Biotechnology for Biofuels* 8 (March): 42.

Saqer, L., M. Al Ahmad, H. Taher, S. Al-Zuhair, and A. H. Al Naqbi. 2015. "Monitoring of Microalgae Lipid Accumulation System Overview." In *2015 IEEE 8th GCC Conference Exhibition*, 1-5.

Schor, Alisha R., and Cullen R. Buie. 2012. "Non-Invasive Sorting of Lipid Producing Microalgae With Dielectrophoresis Using Microelectrodes." *Volume 9: Micro - and Nano-Systems Engineering and Packaging, Parts A and B*. https://doi.org/10.1115/imece2012-88317.

Singh, P., 2014. Applications of Capacitance in monitoring of microbial biofilms. Thapar University, Patiala, India.

Spurr, A. R. 1969. "A Low-Viscosity Epoxy Resin Embedding Medium for Electron Microscopy." *Journal of Ultrastructure Research* 26 (1): 31-43.

Sui, Jianye, Fatima Foflonker, Debashish Bhattacharya, and Mehdi Javanmard. 2020. “Electrical Impedance as an Indicator of Microalgal Cell Health.” *Scientific Reports*. https://doi.org/10.1038/s41598-020-57541-6.

Trainito, Claudia Irene, Olivier Français, and Bruno Le Pioufle. 2015. “Monitoring the Permeabilization of a Single Cell in a Microfluidic Device, through the Estimation of Its Dielectric Properties Based on Combined Dielectrophoresis and Electrorotation in Situ Experiments.” *ELECTROPHORESIS*. https://doi.org/10.1002/elps.201400482.

Trainito, Claudia I., Daniel C. Sweeney, Jaka Čemažar, Eva M. Schmelz, Olivier Français, Bruno Le Pioufle, and Rafael V. Davalos. 2019. “Characterization of Sequentially-Staged Cancer Cells Using Electrorotation.” *PLOS ONE*. https://doi.org/10.1371/journal.pone.0222289.

Uvarov, N. F. 2000. “Estimation of Composites Conductivity Using a General Mixing Rule.” *Solid State Ionics* 136-137 (November): 1267-72.

Valdez-Ojeda, Ruby, Muriel González-Muñoz, Roberto Us-Vázquez, José Narváez-Zapata, Juan Carlos Chavarria-Hernandez, Silvia López-Adrián, Felipe Barahona-Pérez, Tanit Toledano-Thompson, Gloria Garduño-Solórzano, and Rosa María Escobedo-Gracia Medrano. 2015. “Characterization of Five Fresh Water Microalgae with Potential for Biodiesel Production.” *Algal Research* 7 (January): 33-44.

Van Donk, E., M. LÜrling, D. O. Hessen, and G. M. Lokhorst. 1997. “Altered Cell Wall Morphology in Nutrient-Deficient Phytoplankton and Its Impact on Grazers.” *Limnology and Oceanography*. https://doi.org/10.4319/lo.1997.42.2.0357.

Wang, J., V. L. Sukhorukov, C. S. Djuzenova, U. Zimmermann, T. Müller, and G. Fuhr. 1997. “Electrorotational Spectra of Protoplasts Generated from the Giant Marine algaValonia Utricularis.” *Protoplasma* 196 (3-4): 123-34.

Wu, Huawen, Joanne V. Volponi, Ann E. Oliver, Atul N. Parikh, Blake A. Simmons, and Seema Singh. 2011. “In Vivo Lipidomics Using Single-Cell Raman Spectroscopy.” *Proceedings of the National Academy of Sciences of the United States of America* 108 (9): 3809-14.

Wu, Yifan, Chengjun Huang, Lei Wang, Xiaoling Miao, Wanli Xing, and Jing Cheng. 2005. “Electrokinetic System to Determine Differences of Electrorotation and Traveling-Wave Electrophoresis between Autotrophic and Heterotrophic Algal Cells.” *Colloids and Surfaces A: Physicochemical and Engineering Aspects*. https://doi.org/10.1016/j.colsurfa.2005.04.008.

Xu, Xianzhen, Xiaoguang Gu, Zhongyang Wang, William Shatner, and Zhenjun Wang. 2019. “Progress, Challenges and Solutions of Research on Photosynthetic Carbon Sequestration Efficiency of Microalgae.” *Renewable and Sustainable Energy Reviews* 110 (August): 65-82.